Research Article

Zeolite/Cerium Oxide Coat-on Activated Alumina Ball for Arsenite Removal via Fixed-Bed Continuous Flow Adsorption Column

Suttikorn Suwannatrai
Department of Environmental Engineering, Faculty of Engineering, Khon Kaen University, Khon Kaen, Thailand

Dickson Y. S. Yan
Faculty of Science & Technology, The Technological and Higher Education Institute of Hong Kong, New Territories, Hong Kong

Pummarin Khamdahsag
Environmental Research Institute, Chulalongkorn University, Bangkok, Thailand

Visanu Tanboonchuy*
Department of Environmental Engineering, Faculty of Engineering, Khon Kaen University, Khon Kaen, Thailand
Research Center for Environmental and Hazardous Substance Management (EHSM), Khon Kaen University, Khon Kaen, Thailand

* Corresponding author. E-mail: visanu@kku.ac.th DOI: 10.14416/j.asep.2021.11.004
Received: 10 July 2021; Revised: 11 September 2021; Accepted: 1 October 2021; Published online: 5 November 2021

Abstract
Arsenite (As(III)) has threatened human life for ages. It is necessary to remove As(III) from the contaminated water before general use. With the improvement of adsorption, higher As(III) removal can be achieved. This study aimed to develop zeolite/cerium oxide coat-on activated alumina ball adsorbent (CeZ-ball) with the aid of PVA binder and apply it to a fixed-bed continuous flow column for As(III) adsorption. The coating percentage of CeZ-ball was studied. Cerium ions leaching from CeZ-ball were monitored throughout the 2,880-min-column run to confirm the stability of CeZ attached to an activated alumina ball. Surface area, pH point of zero charge, and structural property of CeZ-ball were characterized. An average CeZ coating of 83.3% and rare leaching of cerium proved the coating method. The models proposed by Yoon-Nelson provided the most satisfactory fit with the breakthrough curve ($r^2 = 0.985$, MPSD = 2.547, and $q_0 = 3.481$ mg·g^{-1}) under experimental conditions of the flow rate of 5 mL·min^{-1}, As(III) influent concentration of 1 mg·L^{-1}, and CeZ-ball weight of 40 g. The half-time of breakthrough (τ) was 1,228.739 min. The effects of the key parameters, including initial adsorbent weight, initial flow rate, and initial As(III) concentration, were investigated for the performance of As(III) adsorption. Simulated from the Yoon-Nelson model, the τ increased and the adsorbent weight but decreased as the flow rate increased, thus impacting the As(III) concentration. With the optimal condition, the fixed-bed continuous column with CeZ-ball could be used in As(III) removal from contaminated water.

Keywords: Adsorption, Arsenic, Arsenite, Fixed-bed continuous flow column, Zeolite/cerium oxide

1 Introduction

Arsenic is one of the most important environmental problems, and its current widespread contamination is a serious environmental issue [1], [2]. The two main oxidation states ubiquitous in the nature of arsenic are arsenite [As(III)] and arsenate [As(V)] [3]. Long-term exposure to arsenic causes cancer and skin

lesions. Ultimately, arsenic can accumulate in the skin tissues, lungs, liver, and kidneys through ingestion from contaminated water. Accordingly, both the toxicity and solubility of As(III) in the environment are higher than As(V) [4]–[6].

To eliminate As(III) in water, the development of an efficient method is highly necessary. The adsorption process has high effectiveness, ease of operation, and low-consumption requirements [7], although the efficiency of As(III) removal is currently lower than As(V) [8]. Thus, a pre-oxidation process before the adsorption process appears to be a more effective method than conventional As(III) treatment [9]. However, As(III) detox usually requires oxidizing agents, which leads to the increase of operational costs as well as secondary pollution problems [10]. Thus, it would be productive to develop an adsorbent for high-efficiency in As(III) removal without the requirements of the pre-oxidation process.

In recent years, potential adsorbents, such as Iron (Fe) nanoparticle, Iron oxide nanoparticle (IONP), Zero-valent iron (ZVI), Nano zero-valent iron (N-ZVI), and Fe(III)-modified-MMT have been widely investigated for their effectiveness in arsenic species removal [11]–[13].

Specifically, cerium oxide (CeO_2) has been successful in removing both arsenic species [14]. Earlier, we used CeO_2 for As(III) removal in natural pH, concluding that the adsorption capacity of Langmuir isotherm was 21.27 $mg \cdot g^{-1}$ [15]. However, CeO_2 nanoparticle adsorbents can easily form large aggregate particles [16] and have low ability and adsorption capacity. Preventing this problem involves taking advantage of the smaller particle size, maximizing the active site area, and dispersing the particles to increase adsorption capacity.

Consequently, Na-P Zeolite is considered a good adsorbent for As(V) removal (≥ 60%), and it can be a good material to use as a supporter for adsorbent materials [17] and to help eliminate arsenic residue in solutions [18], [19]. Therefore, Na-P zeolite will be utilized for protection against CeO_2 nanomaterial aggregation during the oxidation process and help eliminate As(V) from this process. From real field adsorption processes, the powder form of materials due to the separation difficulty fails the blockage and gets clogged in the column [20]. Thus, it is necessary to pelletize the sorbents to prevent possible problems. An activated alumina ball is also a popular material to support and prevent a clogged column. Therefore, it is important to pelletize and examine the actual adsorbent performance in terms of optimal adsorption capacity and the half time of the breakthrough curve.

To address the gap, the objectives of this study are 1) to pelletize the zeolite/cerium oxide (CeZ) with activated alumina ball by polyvinyl alcohol (PVA) binders for a fixed-bed column experiment, 2) to analyze the column behavior of As(III) adsorption in a continuous fixed-bed column, and 3) to estimate the parameters controlling the breakthrough behavior (initial adsorbent weight, initial flow rate, and initial As(III) concentration). The Adams-Bohart, Thomas, and Yoon-Nelson models were applied to predict the breakthrough behavior and used the best model to simulate the parameters controlling the operational conditions.

2 Experimental

2.1 *Materials and preparation of CeZ-ball*

All chemicals were analytical grade reagents and were used as received, without further purification. The stock solution of arsenite containing 1,000 $mg \cdot L^{-1}$ was prepared using $NaAsO_2$ (90%, Merck, Germany), ready for preparing As(III) influent concentration. All solutions were prepared with RO water (1.178 $\mu S \cdot cm^{-1}$). An activated alumina ball ($Al_2O_3 \cdot nH_2O$) with a diameter size of 3–5 mm (HYAA300, E.D.S. International, Thailand) was employed to support the coating process.

The CeZ was prepared by mixing 1 g Na-P zeolite [19] in 50 mL of 1 M NaOH (97%, Merck, Germany) and 3.1 g of $Ce(NO_3)_3.6H_2O$ (99%, Merck, Germany) in 10 mL of RO water. The mixing solution was stirred for 30 min in an ambient environment. The resulting precipitate product was centrifuged and washed with the excess remnants of RO water. After that, the residues were dried at 105 °C for 24 h and calcined in an electric furnace at 250 °C for 12 h.

The CeZ-ball was prepared by coating the CeZ powder on activated alumina balls using a mechanical orbital shaker (Shaking Water Bath WNB 22, Memmert, Germany) with a binder. The weight ratio of CeZ powder and activated alumina balls were 0.5: 20 g. Firstly, the activated alumina balls were introduced

to a 250 mL flask, dropping a 5 mL of 10 w/v% polyvinyl alcohol (PVA) (98.99%, Loba Chemie, India) in RO water into them. The mixtures in the flask were gently shaken by hand to let the PVA binder cover the balls. Then, the CeZ powder was added to the flask. They were transferred to an orbital shaker at 160 rpm for 6 h under 27–28 °C. After that, the CeZ-ball was dried at 105 °C for 24 h. Finally, the CeZ-ball was ready for packing into continuous fixed-bed

2.2 *Characterization of CeZ-ball adsorbent*

The pH_{pzc} was determined by the salt addition method. Initially, 40 mL of NaCl (0.01 M) was placed in several closed flasks. The pH within each flask was adjusted to a value between 3 to 12 using 0.01 M NaOH and 0.01 HCl. Then, 0.1 g of materials were added to each flask and agitated for 48 h. The final pH was measured [21].

The specific surface area in the CeZ and CeZ-ball was measured by the Brunauer-Emmett-Teller (BET) method (TriStar II 3020, Micromeritics, USA) using nitrogen as the adsorbate.

The crystal structure of the CeZ and CeZ-ball was characterized by an XRD (D8 Discover, Bruker AXS, Germany). The XRD patterns were collected with a scan range of 20–80° using Cu Kα radiation (λ = 0.1514 nm) at 40 kV and 40 mA.

2.3 *Fixed-bed continuous flow adsorption experiment*

A fixed-bed continuous flow experiment was conducted to evaluate the behavior of As(III) removal from solutions and the cerium leaching test. Experiments in these studies were done with a glass tube having an internal diameter of 2.0 cm and 20 cm height. 40 g (15-cm-long bed) of CeZ-ball was packed into the glass tube between the bottom and up of thick glass beads and cotton wool to avoid any out-off (Figure 1).

The experiments duplicate performed using the important parameters such as 5 $mL \cdot min^{-1}$ of flow rate, 1 $mg \cdot L^{-1}$ of As(III) influent concentration, and 40 g (15-cm-long bed) of CeZ-ball were closely investigated. The As(III) solution was pumped using a peristaltic pump (up-flow mode through the column). The arsenic concentrations were examined by ICP-OES (PerkinElmer Optima 8000).

The effects of the important parameters were

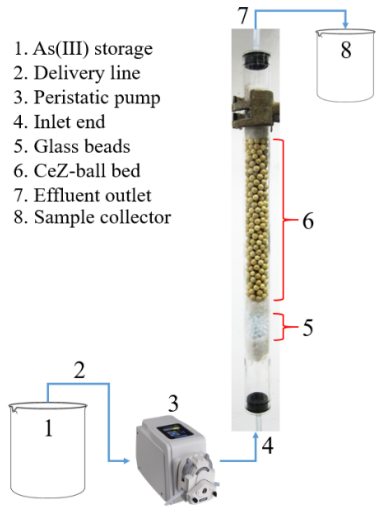

Figure 1: Experimental setup for fixed-bed continuous flow study.

realized with flow rate into the column (3, 5, 7.5 and 10 $mL \cdot min^{-1}$), the weight of adsorbent (0.5, 1, 1.5 and 2 g), and initial As(III) concentrations (1, 1.5, 2 and 3 $mg \cdot L^{-1}$) were calculated by the predictive model.

The experimental data can be used to calculate kinetic constants from a suitable model. The breakthrough curve showed the performance of the adsorption efficiency of the column. Breakthrough time and shape are important parameter data for fixed-bed column operation [22]. The plot of the breakthrough curve used effluent concentration to the inlet concentration (C_t/C_0) as a function of time (t) or bed volume (BV). In this study, the breakthrough behavior, capacity, and breakthrough time were analyzed using the three models.

2.4 *Mathematical modeling of fixed-bed column experiment*

The models were developed to analyze, predict behaviors, and calculate the kinetic parameters, and utilized to determine the performance of the fixed-bed column. The three mentioned models are detailed as follows:

The Thomas model was applied to achieve the experimental data of the fixed-bed continuous column studied. This model assumes that the adsorption behavior follows Langmuir isotherm without axial dispersion and second-order reaction kinetic [23], [24]. The Thomas equation is presented as Equation (1):

$$\frac{C}{C_0}=\frac{1}{1+exp\left(\frac{k_{Th}(q_0 m-C_0 V_{eff})}{Q}\right)} \quad (1)$$

The linear form is expressed as Equation (2) [18]:

$$ln\left(\frac{C_0}{C_t}-1\right)=\frac{k_{Th}q_0 m}{Q}-k_{Th}C_0 t \quad (2)$$

where k_{Th} is the Thomas rate constant (mL·min^{-1}·mg^{-1}), Q is the flow rate (mL·min^{-1}), m is the amount of adsorbent in the column (g), q_0 is the equilibrium adsorption capacity (mg·g^{-1}), C_0 and C_t are the As(III) concentration in the influent and at the time, respectively (mg·L^{-1}). The linear plot of ln[(C_0/C_t) –1] versus t gives the value of k_{TH}, q_0, and R^2 are shown in Table 2.

Yoon-Nelson developed a relatively simple model that requires no detailed characteristics of the adsorbate, type of adsorbent, and properties of adsorption bed data in the column. This model assumes that the absorbate molecule is proportional to the probability of the adsorbate adsorption and the probability of adsorbate breakthrough on the adsorbent [24]. This equation is presented as Equation (3):

$$\frac{C}{C_0}=\frac{exp\left[K_{YN}(t-\tau)\right]}{1+exp\left[K_{YN}(t-\tau)\right]} \quad (3)$$

The linear form can be summarized as Equation (4) [25], [26]:

$$ln\left(\frac{C_t}{C_0-C_t}\right)=k_{YN}t-\tau k_{YN} \quad (4)$$

The equilibrium adsorption capacity (q_0) can be estimated using Equation (5) as follows:

$$q_0=\frac{C_0 Q\tau}{m} \quad (5)$$

where k_{YN} is the Yoon-Nelson rate constant (min^{-1}), τ is the time required for 50% of the adsorbate (min), Q is the flow rate (mL·min^{-1}), C_0 and C_t are the As(III) concentrations in the influent and at time t, respectively (mg·L^{-1}), and q_0 is the equilibrium adsorption capacity (mg·g^{-1}). The linear plot of (C_t/(C_0 – C_t)) versus t gives the value of k_{YN}, τ, and R^2 are shown in Table 2.

The Adams-Bohart model assumes that the adsorption rate is proportional to the concentration of the adsorbing individual and to the residual capacity of the adsorbent. The model is applied to analyze 10–50% of the saturation point [27]. The equation is expressed as Equations (6) and (7) [28] as follows:

$$\frac{C}{C_0}=\frac{exp(k_{AB}C_0 t)}{exp\left(\frac{k_{AB}N_0 L}{\upsilon}\right)-1+exp(k_{AB}C_0 t)} \quad (6)$$

The linear form is:

$$ln\left(\frac{C_t}{C_0}\right)=k_{AB}C_0 t-k_{AB}N_0\left(\frac{Z}{\upsilon}\right) \quad (7)$$

where k_{AB} is the mass transfer coefficient (L·mg^{-1}·min^{-1}), Z is the bed depth (cm), υ is the superficial velocity (cm·min^{-1}), N_0 is the saturation adsorption capacity per column volume (mg·L^{-1}). C_0 and C_t are the As(III) concentrations in the influent and effluent at time t, respectively (mg·L^{-1}). The linear plot of ln(C_t/C_0) versus t gives the k_{AB}, υ, and R^2 shown in Table 2. The value of k_{AB} decreases, yet the concentration and flow rate is increased, corresponding to the increase of bed depth.

3 Results and Discussion

3.1 *Characterization of CeZ-ball adsorbent*

As shown in Figure 2, the pellets were collected as fresh activated alumina ball (a), and the CeZ-ball was dried at 105 °C for 24 h (b). Table 1 shows the percentage coating of CeZ on the activated alumina ball surface. The surface of the activated alumina ball detected CeZ material up to approximately 83.3% (average 0.416 g CeZ coating on Al_2O_3 ball the surface). However, some PVA and CeZ were stuck on the flask surface. It could be presumed that the loss of material was around 16.7%.

Table 1: Percentage of CeZ on the surface of activated alumina (Al_2O_3) ball

Batch no.	Al_2O_3 Ball Weight (g)	CeZ-ball Weight (g)	%Coating
1	20.168	20.610	88.4
2	20.112	20.502	78.0
3	20.032	20.450	83.6
Average			83.3

Figure 3 shows the leaching test in a fixed-bed continuous adsorption column compared to the Ce ion concentration at different times. There was the rare dissolving of Ce ions in the solution throughout

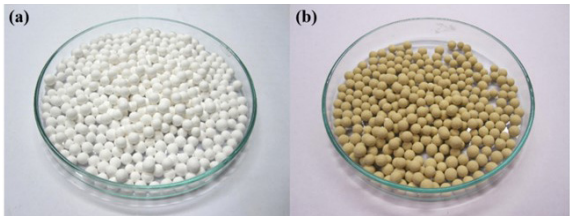

Figure 2: (a) Activated alumina ball, and (b) CeZ-ball.

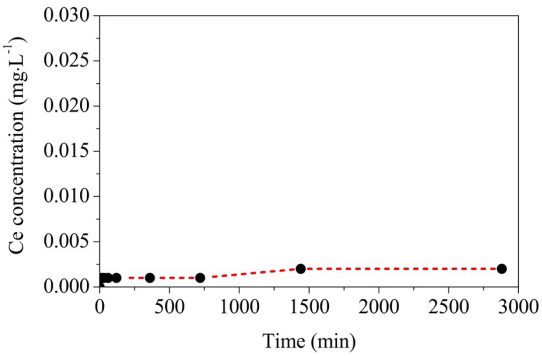

Figure 3: Cerium leaching test in a fixed-bed continuous adsorption column (experimental conditions: CeZ-ball 10 g, pH 7.5 ± 0.2, and 28 °C).

10 to 2,880 min. Thus, the PVA was considered a perfect compound as it could preserve CeZ on the surface of the activated alumina ball. CeZ-ball stabilization could be maintained along the run.

The point of zero charges (pH_{pzc}) can be evaluated by the pH value, which is the net charge of the total particle surface equal to zero [21]. Figure 4 shows the plot of the final pH of CeZ and CeZ-ball as a function of initial pH in the solution. The pH_{pzc} values of CeZ showed a more positive surface than CeZ-ball, which were found to be approximately 9.5 and 7.2, respectively. These results indicate that the CeZ-ball is positively charged, while the surface of the CeZ-ball has a positive charge beyond a pH 7.2; at pH greater than 7.2, while that is negative the surface. The species of As(III) existed predominantly as H_3AsO_3 and H_2AsO_3- below 9.2, whereas the surfaces are negatively charged at pH > pH_{pzc} and As anions adsorption is suppressed due to electrostatic repulsion [10].

The surface area of the material was obtained using the Brunauer-Emmett-Teller (BET) method. BET analysis indicated that the surface area decreased after coating from 224.6 to 202.3 $m^2 \cdot g^{-1}$. Because the PVA may cover the surface of CeZ, it leads to surface

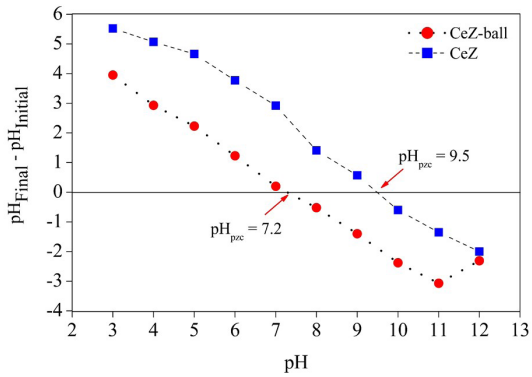

Figure 4: pH point of zero charge (pH_{pzc}) of CeZ, and CeZ-ball.

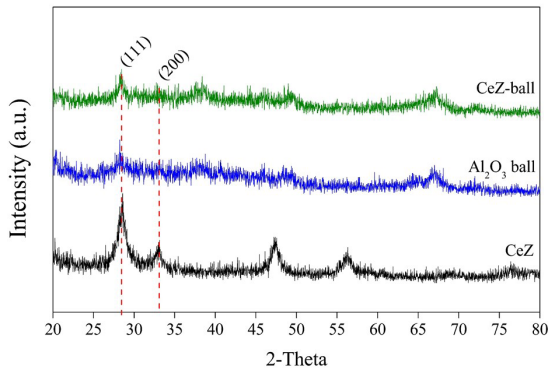

Figure 5: XRD patterns of Al_2O_3 ball, CeZ, and CeZ-ball.

area decreases.

X-ray diffraction (XRD) is used to study the structural properties and detect elemental factors on the surface of a material. The pattern of CeZ and CeZ-ball is shown in Figure 5. All the XRD profiles material exhibit the main peak at 2θ = 28.5 and 33.0, corresponding to (111) and (200) crystal plane for CeO_2. This peak indicates the crystalline nature of CeZ and signifies the structure of CeZ dispersion on the surface of the activated alumina ball.

3.2 *Modeling of the breakthrough curve*

The breakthrough curve at the C/C_0 vertical position was compared with the time point. The results are used according to 40 g of adsorbent weight (0.833 g of CeZ), 1.0 $mg \cdot L^{-1}$ of As(III) influent concentration, and 5 $mL \cdot min^{-1}$ of flow rate. The constant effluent flow rate indicated that clogging did not occur in the

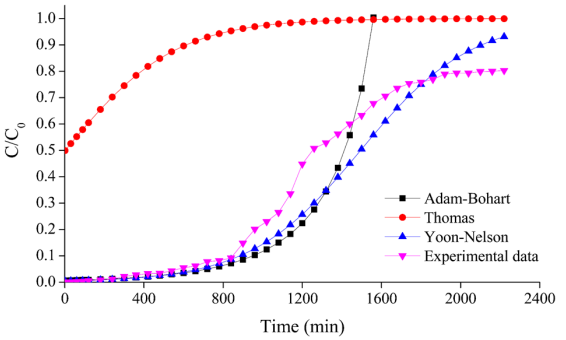

Figure 6: Application of models for As(III) removal (experimental conditions: flow rate 5 mL·min^{-1}, As(III) influent concentration 1 mg·L^{-1}, CeZ-ball 40 g, and pH 6.5±0.2).

column. In addition, there was likely to be no adsorption of As(III) on the activated alumina ball. Therefore, it was revealed that the As(III) adsorption achieved a full removal process due to CeZ. The breakthrough curve of As(III) on CeZ-ball adsorption is presented in Figure 6. The breakthrough point of the CeZ-ball column was about 800 min, while the exhaustion point was about 2,000 min.

3.3 *Error analysis*

From Figure 6 and linear regression coefficient (r^2), both models between the Thomas and Yoon-Nelson provided a better application for data collection [29]. However, Marquardt's standard deviation (*MPSD*) was employed to find the best-fitted model. It is the most suitable optimization method for evaluating the best models between the Thomas and Yoon-Nelson models [30]. The equation is given below as Equation (8) [31]:

$$PSD = \sqrt{\frac{1}{p-n}\sum_{i-1}^{p}\left(\frac{(q_{Exp}-q_{Pre})}{q_{Exp}}\right)^2} \quad (8)$$

where n is the number of parameters in the model, p is the amount of experimental data, and q_{Exp} and q_{Pre} refer to the experimental and predicted values from the model, respectively.

The obtained parameters of the three models are also listed in Table 2. This was further supported by a high value of r^2 and *MPSD*, indicating that the column adsorption data best aligned with the Yoon-Nelson model (*MPSD* = 2.547) and was well applicable in analyzing the column adsorption data [32]. The results indicate that the molecule of As(III) is proportional to the probability of the As(III) adsorption and the probability of As(III) breakthrough on the CeZ-ball [31]. The half time of the breakthrough curve (τ) of As(III) on the CeZ-ball adsorption column was shown as 1,228.739 min. The Thomas model predicted a maximum adsorption capacity of CeZ-ball (q_0) = 3.482 mg·g^{-1}.

Table 2: Parameters and results of column adsorption from fitting data with a comparison of the three models

Model	Parameters		*MPSD*
Adam-Bohart	k_{BA}, L·mg^{-1}·min^{-1}	0.003	6.700
	N_0, mg·L^{-1}	369.127	
	r^2	0.855	
Yoon-Nelson	k_{YN}, min^{-1}	0.005	2.547
	τ, min	1,228.739	
	q_0, mg·g^{-1}	3.481	
	r^2	0.985	
Thomas	k_{TH}, L·min^{-1}·mg^{-1}	0.005	496.319
	q_0, mg·g^{-1}	3.482	
	r^2	0.985	

3.4 *Effect of adsorbent weights*

The breakthrough curves of As(III) ions adsorption by CeZ-ball at the different packing weights is presented in Figure 7. The flow rate and As(III) concentration were fixed at 5 mL·min^{-1} and 1 mg·L^{-1}, respectively. Moreover, the weight of CeZ in the CeZ-ball in the bed varied according to the experimental data (based on 40 g of CeZ-ball or 0.833 g of CeZ) and the fitting equation from Yoon-Nelson models at 0.5, 1.0, 1.5, and 2.0 g of CeZ. Figure 7 indicates the breakthrough and exhaustion time of As(III) adsorption were delayed with the increase in the weight of CeZ-ball. The half time of breakthrough of adsorption increased from 409.580 to 1,638.319 min with the increased weight of CeZ from 0.5 to 2.0 g (Table 3). It is illustrated that increasing the weight of the CeZ-ball is very important for the column process. The performance of the column was improved with the weight of the CeZ-ball because more CeZ-ball was packed in the fixed-bed column, which provided greater adsorption sites for As(III) ions. Thus, the longer residence time of As(III) ions in the column caused better intra-particle phenomena.

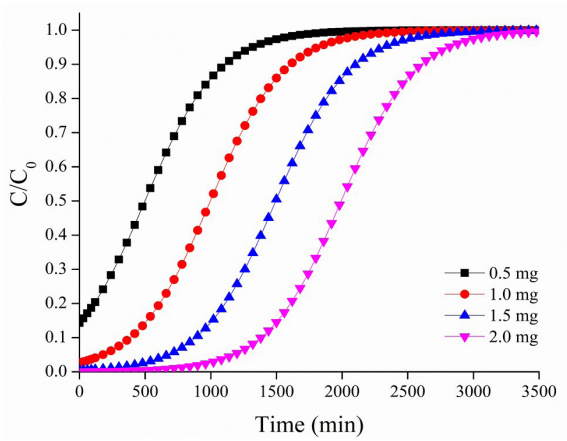

Figure 7: Effect of adsorbent weight on the breakthrough curve of As(III) adsorption.

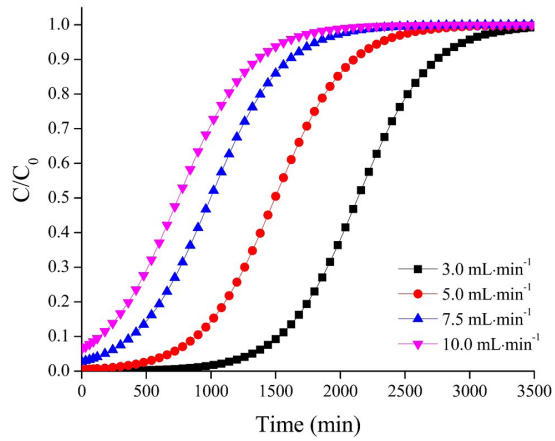

Figure 8: Effect of initial flow rate on the breakthrough curve of As(III) adsorption.

3.5 *Effect of flow rates*

The flow rate is a necessary parameter of the continuous process, especially in wastewater operation, because the flow rate controls the equilibrium of adsorption or is always affected by the contact time, which is determined by the flow rate. In this experiment, the CeZ-ball packing weight and As(III) concentration in the column were fixed at 40 g and 1.0 mg·L^{-1}, respectively. The initial flow rates were varied to 3.0, 5.0, 7.5, and 10 mL·min^{-1}.

The breakthrough curve of the varied flow rate simulated from the Yoon-Nelson model is depicted in Figure 8. As a result, the deterioration time was reduced for As(III) adsorption with the increased flow rate. The half time of breakthrough of adsorption decreased from 2,047.899 to 614.373 min, with the increase of the flow rate from 3.0 to 10.0 mL·min^{-1} (Table 3). Also, when increasing the flow rates were observed that the breakthrough curve will be steeper. This was due to the effect of solute diffusion on the surface of the CeZ-ball caused by the increased flow rate. Since As(III) has less contact time of diffusion at the surface of the CeZ-ball, at the lower flow rate, the As(III) needed more time at contact with CeZ, resulting from the higher removal of As(III) from the solution.

This result indicates that a low flow rate provides sufficient contact time of adsorbate to reach equilibrium. Thus, the As(III) ions have more contact time with CeZ-ball in the column. Also, this allows enough time for As(III) ions to diffuse into the pores of CeZ through intraparticle diffusion.

3.6 *Effect of As(III) influent concentrations*

The results from the effects of As(III) influent concentration on the breakthrough curve calculated by using the obtained Yoon-Nelson model equation are shown in Figure 9. The flow rate and packing weights of the adsorbent are defined at 5 mL·min^{-1} and 40 g, respectively. The initial As(III) concentrations were determined at 1.0, 1.5, 2.0, and 3.0 mg·L^{-1}, respectively.

From Figure 9, the half time of breakthrough was decreased as the increase of the initial As(III) concentration occurred. The breakthrough curves were steeped with increased initial As(III) concentration, and the breakthrough occurred faster. The half time of breakthrough for As(III) adsorption decreased

Table 3: Comparison of predicted key parameters from the Yoon-Nelson model

CeZ (g)	τ (min)	Flow rate (mL·min^{-1})	τ (min)	[As(III)] (mg·L^{-1})	τ (min)
0.5	409.580	3.0	2,047.899	1.0	1,044.428
1.0	819.159	5.0	1,228.739	1.5	696.286
1.5	1,228.739	7.5	819.159	2.0	522.214
2.0	1,638.319	10.0	614.370	3.0	348.143

Table 4: Comparison of the dynamic adsorption parameters for arsenic removal with various adsorbents

Adsorbent	Z (cm)	Q (mL·min^{-1})	C (mg·L^{-1})	pH	Temp (°C)	τ (min)	q_0 (mg·g^{-1})	Ref.
Chitosan	13.0	2	120	8	21	446.5	46.5	[29]
	13.2	2	60	8	21	832.8	43.3	[29]
Iron oxide-coated cement (IOCC)	10	8.5	0.5	-	27 ± 2	1411.7	0.247	[33]
	10	4.3	1.35	-	27 ± 2	1131.2	0.279	[33]
Bismuth-impregnated aluminum oxide (BiAl)	-	20	1	-	25	-	15.65	[34]
Magnetic honeycomb briquette cinders composite (MHBC)	-	540	0.3	7.1	-	-	24.24	[35]
Multi walled carbon nanotube (CNTs), powder	25	30	40	6	25	-	0.0135	[36]
CeZ ball	15	5	1	6.5 ± 2	28 ± 2	1228.7	3.481	This study

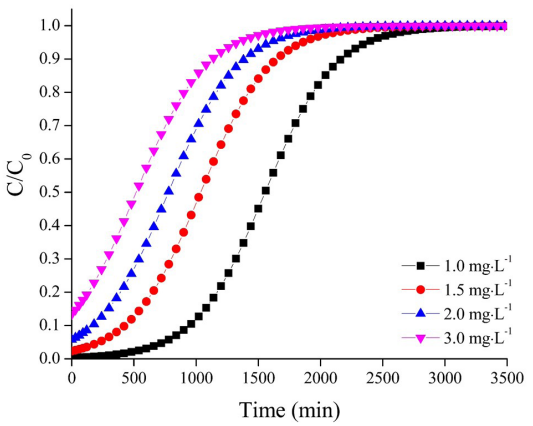

Figure 9: Effect of As(III) influent concentration on the breakthrough curve of As(III) adsorption.

from 1,044.428 to 348.143 min as the initial As(III) concentration increased from 1.0 to 3.0 mg·L^{-1} (Table 3). A comparison of the dynamic adsorption parameters with various adsorbents is shown in Table 4.

Also, a higher As(III) influent concentration accelerated the exhaustion of the column. It can be assumed that the higher the As(III) concentration grew, the stronger the driving force occurred in adsorption. This pointed to the higher concentration increasing the diffusion coefficient, leading to faster transportation. Hence, the adsorbent (CeZ) in the column achieved quicker saturation.

4 Conclusions

CeZ was pelletized with an activated alumina ball by PVA binder, which found that the CeZ on the surface of the activated alumina ball increased up to 83.3%. The CeZ-ball was performed in a fixed-bed column. The Yoon-Nelson model is considered the most precise model to describe the breakthrough curves (*MPSD* = 2.547 and q_0 = 3.481 mg·g^{-1}). This model illustrated the half-time of breakthrough (τ) at 1,228.739 min. The application of the Yoon-Nelson model showed that the τ increased along with the adsorbent weight but decreased with increased flow rate and As(III) concentration.

Acknowledgments

This study was supported by Research and Graduate Studies, Khon Kaen University, Khon Kaen, Thailand.

References

[1] Y. Xiong, Q. Tong, W. Shan, Z. Xing, Y. Wang, and S. Wen, "Arsenic transformation and adsorption by iron hydroxide/manganese dioxide doped straw activated carbon," *Applied Surface Science*, vol. 416, pp. 618–627, 2017.

[2] Z. Wen, Y. Zhang, X. Zhou, and R. Chen, "Effective As(III) and As(V) immobilization from aqueous solution by nascent ferrous hydroxide colloids (FHC)," *Separation and Purification Technology*, vol. 176, pp. 395–401, 2017.

[3] R. Yadav, A. K. Sharma, and J. N. Babu, "Sorptive removal of arsenite [As(III)] and arsenate [As(V)] by fuller's earth immobilized nanoscale zero-valent iron nanoparticles (F-nZVI): Effect of Fe^0 loading on adsorption activity," *Journal of Environmental Chemical Engineering*, vol. 4, no. 1, pp. 681–694, 2016.

[4] C. Zihang, F. Fu, D. D. Dionysiou, and B. Tang, "Adsorption, oxidation, and reduction behavior of arsenic in the removal of aqueous As(III) by mesoporous Fe/Al bimetallic particles," *Water Research*, vol. 96, pp. 22–31, 2016.

[5] H. Zongliang, S. Tian, and N. Ping, "Adsorption of arsenate and arsenite from aqueous solutions by cerium-loaded cation exchange resin," *Journal of Rare Earths*, vol. 30, no. 6, pp. 563–572, 2012.

[6] A. Sadiya, S. Shafinaz, I. Norahim, J. N. Mohammed, D. V. N. Vo, and F. A. Manan, "Arsenic removal technologies and future trends: A mini review," *Journal of Cleaner Production*, vol. 278, p. 123805, 2021.

[7] D. Liu, S. Deng, A. Maimaiti, B. Wang, J. Huang, Y. Wang, and G. Yu, "As(III) and As(V) adsorption on nanocomposite of hydrated zirconium oxide coated carbon nanotubes," *Journal of Colloid and Interface Science*, vol. 511, pp. 277–284, 2018.

[8] G. Zhang, J. Qu, H. Liu, R. Liu, and R. Wu, "Preparation and evaluation of a novel Fe-Mn binary oxide adsorbent for effective arsenite removal," *Water Research*, vol. 41, no. 9, pp. 1921–1928, 2007.

[9] B. Rathi, J. Jamieson, J. sun, A. J. Siade, M. Zhu, O. A. Cirpka, and H. Prommer, "Process-based modeling of arsenic(III) oxidation by manganese oxides under circumneutral pH conditions," *Water Research*, vol. 185, 2020, Art. no. 11695.

[10] L. Zhang, T. Zhu, X. Liu, and W. Zhang, "Simultaneous oxidation and adsorption of As(III) from water by cerium modified chitosan ultrafine nanobiosorbent," *Journal of Hazardous Materials*, vol. 308, pp. 1–10, 2016.

[11] M. Biterna, L. Antonoglou, E. Lazou, and D. Voutsa, "Arsenite removal from waters by zero valent iron: Batch and column tests," *Chemosphere*, vol. 78, no. 1, pp. 7–12, 2010.

[12] D. Dickson, G. Liu, and Y. Cai, "Adsorption kinetics and isotherms of arsenite and arsenate on hematite nanoparticles and aggregates," *Journal of Environmental Management*, vol. 186, pp. 261–267, 2017.

[13] C. Luengo, V. Puccia, and M. Avena, "Arsenate adsorption and desorption kinetics on a Fe(III)-modified montmorillonite," *Journal of Hazardous Materials*, vol. 186, no. 2–3, pp. 1713–1719, 2011.

[14] W. Sun, Q. Li, S. Gao, and J. K. Shang, "Exceptional arsenic adsorption performance of hydrous cerium oxide nanoparticles: Part B. Integration with silica monoliths and dynamic treatment," *Chemical Engineering Journal*, vol. 185–186, pp. 136–143, 2012.

[15] S. Suwannatrai, D. Y. S. Yan, J. Phanthasri, P. Khamdahsag, S. Wannapaiboon, and V. Tanboonchuy, "Oxidation-adsorption of arsenite contaminated water over ceria nanorods," *Desalination and Water Treatment*, vol. 200, pp. 252–261, 2020.

[16] Y. L. Yang, Y. J. Li, Y. H. Yuan, R. P. Liang, and J. D. Qiu, "Target induced aggergation of Ce(III)-based coordination polymer nanoperticles for fluorimertric detection of As(III)," *Talanta*, vol. 190, pp. 255–262, 2018.

[17] Z. Li, L. Wang, J. Meng, X. Liu, J. Xu, and F. Wang, "Zeolite-supported nanoscale zero-valent iron: New findings on simultaneous adsorption of Cd(II), Pb(II), and As(III) in aqueous solution and soil," *Journal of Hazardous Materials*, vol. 344, pp. 1–11, 2018.

[18] J. Phanthasri, N. Grisdanurak, P. Khamdahsag, K. Wantala, R. Khunphonoi, S. Wannapaiboon, and V. Tanboonchuy, "Role of zeolite-supported nanoscale zero-valent iron in selenate removal," *Water, Air, and Soil Pollution*, vol. 231, no. 5, pp. 1–12, 2020.

[19] W. Chansiriwat, D. Tanangteerapong, and K. Wantala, "Synthesis of zeolite from coal fly ash by hydrothermal method without adding alumina and silica sources: Effect of aging temperature and time," *Sains Malaysiana*, vol. 45, no. 11, pp. 1723–1731, 2016.

[20] H. Yin, M. Kong, X. Gu, and H. Chen, "Removal of arsenic from water by porous charred granulated attapulgite-supported hydrated iron oxide in bath and column modes," *Journal of Cleaner Production*, vol. 166, pp. 88–97, 2017.

[21] S. Cheng, L. Zhang, A. Ma, H. Xia, J. Peng, C. Li, and J. Shu, "Comparison of activated carbon and iron/cerium modified activated carbon to remove methylene blue from wastewater," *Journal of Environmental Science*, vol. 5, pp. 1–11, 2017.

[22] S. Chen, Q. Yue, B. Gao, Q. Li, X. Xu, and K. Fu, "Adsorption of hexavalent chromium from aqueous solution by modified corn stalk: A fixed-

bed column study," *Bioresource Technology*, vol. 113, pp. 114–120, 2012.

[23] H. C. Thomas, "Heterogeneous ion exchange in a flowing system," *Journal of the American Chemical Society*, vol. 66, no. 10, pp. 1664–1666, 1944.

[24] P. Dhanasekaran, P. M. S. Sai, and K. I. Gnanasekar, "Fixed bed adsorption of fluoride by Artocarpus hirsutus based adsorbent," *Journal of Fluorine Chemistry*, vol. 195, pp. 37–46, 2017.

[25] Y. Dong and H. Lin, "Competitive adsorption of Pb(II) and Zn(II) from aqueous solution by modified beer lees in a fixed bed column," *Process Safety and Environmental Protection*, vol. 1, no. 111, pp. 263–269, 2017.

[26] M. Trgo, N. V. Medvidović, and J. Perić, "Application of mathematical empirical models to dynamic removal of lead on natural zeolite clinoptilolite in a fixed bed column," *Indian Journal of Chemical Technology*, vol. 18, no. 2, pp. 123–131, 2011.

[27] J. Cruz-Olivares, C. Pérez-Alonso, C. Barrera-Díaz, F. Ureña-Nuñez, M. C. Chaparro-Mercado, and B. Bilyeu, "Modeling of lead(II) biosorption by residue of allspice in a fixed-bed column," *Chemical Engineering Journal*, vol. 228, pp. 21–27, 2013.

[28] Y. Long, D. Lei, J. Ni, Z. Ren, C. Chen, and H. Xu, "Packed bed column studies on lead(II) removal from industrial wastewater by modified Agaricus bisporus," *Bioresource Technology*, vol. 152, pp. 457–463, 2014.

[29] R. Brion-Roby, J. Gagnon, J. S. Debastien, and B. Chabot, "Investigation of fixed bed adsorption column operation parameters using a chitosan material for treatment of arsenate contaminated water," *Journal of Environmental Chemical Emgineering*, vol. 6, pp. 505–511, 2018.

[30] M. V. Sergio, I. M. Arturo, E. H. B. Elias, F. M. R. Oscar, V. H. Virgilio, P. C. Cristobal, and L. L. Jaime, "As(III) and As(V) adsorption on manganese ferrite nanoparticles," *Journal of Molecular Structure*, vol. 1154, pp. 524–534, 2018.

[31] F. Fadzil, S. Ibrahim, and M. A. K. M. Hanafiah, "Adsorption of lead(II) onto organic acid modified rubber leaf powder: Batch and column studies," *Process Safety and Environmental Protection*, vol. 100, pp. 1–8, 2016.

[32] D. Jiang, Y. Amano, and M. Machida, "Removal and recovery of phosphate from water by a magnetic Fe_3O_4 @ASC adsorbent," *Journal of Environmental Chemical Engineering*, vol. 5, no. 5, pp. 4229–4238, 2017.

[33] S. Kundu and A. K. Gupta, "As(III) removal from aqueous medium in fixed bed using iron oxide-coated cement (IOCC): Experimental and modeling studies," *Chemical Engineering Journal*, vol.129, pp. 123–131, 2007.

[34] N. Zhu, J. Qiao, Y. Ye, and T. Yan, "Synthesis of mesoporous bismuth-impregnated aluminum oxide for arsenic removal: Adsorption mechanism study and application to a lab-scale column," *Journal of Environmental Management*, vol. 211, pp.73–82, 2018.

[35] S. A. Baig, J. Zhu, L. Tan, X. Xue, C. Sun, and X. Xinhua, "Influence of calcination on magnetic honeycomb briquette cinders composite for the adsorptive removal of As(III) in fixed-bed column," *Chemical Engineering Journal*, vol. 257, pp. 1–9, 2014.

[36] I. Ali, "Microwave assisted economic synthesis of multi walled carbon nanotubes for arsenic species removal in water: Batch and column operation," *Journal of Molecular Liquids*, vol. 271, pp. 677–685, 2018.